Influence of magnetism on vertical hopping transport in CrSBr

Xiaohanwen Lin,[1,2] Fan Wu,[1,2] Sara A. López-Paz,[1] Fabian O. von Rohr,[1] Marco Gibertini,[3,4] Ignacio Gutiérrez-Lezama,[1,2] and Alberto F. Morpurgo[1,2,*]

[1]*Department of Quantum Matter Physics, University of Geneva, 24 Quai Ernest Ansermet, CH-1211 Geneva, Switzerland*
[2]*Department of Applied Physics, University of Geneva, 24 Quai Ernest Ansermet, CH-1211 Geneva, Switzerland*
[3]*Dipartimento di Scienze Fisiche, Informatiche e Matematiche, University of Modena and Reggio Emilia, I-41125 Modena, Italy*
[4]*Centro S3, CNR Istituto Nanoscienze, I-41125 Modena, Italy*

(Received 23 August 2023; revised 8 December 2023; accepted 18 January 2024; published 20 February 2024)

We investigate the *c*-direction conduction in CrSBr in the linear regime, which is not accessible in other van der Waals (vdW) magnetic semiconductors, because of the unmeasurably low current. The resistivity, which is 10^8-10^{11} times larger than in the *a* and *b* directions, exhibits magnetic state dependent thermally activated and variable range hopping transport. In the spin-flip phase at 2 T, the activation energy is 20 meV lower than in the antiferromagnetic state due to a downshift of the conduction band edge, in agreement with *ab initio* calculations. In the variable range hopping regime, the average hopping length decreases from twice the interlayer distance to the interlayer distance at 2 T because in the antiferromagnetic state the large exchange energy impedes electrons hopping between adjacent layers. Our work demonstrates that the linear transport regime provides new information about electronic processes in vdW magnetic semiconductors and shows how magnetism influences these processes both in real and reciprocal space.

DOI: 10.1103/PhysRevResearch.6.013185

I. INTRODUCTION

Temperature and magnetic field dependent transport measurements provide a powerful approach to mapping the magnetic phase diagram of two-dimensional magnetic semiconductors (2DMSs) [1–5]. In most cases, measurements rely on devices with electrodes attached on opposite sides of a multilayer to probe the current flowing perpendicular to the layers [4–15]. The resulting current-voltage (I-V) curves commonly exhibit a characteristic strong nonlinearity, with $\ln(I/V^2)$ scaling proportionally to $1/V$ at high bias, a dependence usually interpreted in terms of a Fowler-Nordheim (FN) tunneling scenario [see Fig. 1(a)] [16,17]. In its usual form, however, FN tunneling theory assumes electrons have a quadratic dispersion relation up to energies much higher than the barrier height, an assumption invalid for most 2DMSs explored so far because of their extremely narrow bandwidths [18,19]. Interpreting experiments in terms of FN tunneling should therefore be considered as a useful phenomenological approach, with the microscopic electronic processes responsible for vertical transport in 2D magnetic semiconductors remaining to be identified.

Gaining a deeper understanding of these microscopic processes experimentally is difficult because most multilayers of 2DMSs are so resistive that the current in the linear I-V transport regime, which is simpler to interpret than the nonlinear one, is too small to detect [4,5,11,15]. Even though for truly atomically thin layers linear transport due to direct tunneling is observed, current in the linear transport regime becomes unmeasurably small for barriers that are only a few monolayers thick. To probe more effectively the microscopic transport processes in 2DMSs and their interplay with the magnetic state, materials are needed in which linear transport can be measured in a broad range of temperatures and magnetic fields to test whether the evolution of the conductivity can be properly described in terms of processes well-understood in conventional semiconductors.

Here, we report on vertical transport experiments on CrSBr exfoliated layers with different thicknesses, in which the linear regime is detected over a broad range of temperatures and magnetic fields. We find that the linear resistance increases in a thermally activated way [$R = R_0 \exp(\frac{E_a}{kT})$; see Fig. 1(a)] between room temperature and approximately 60 K, before crossing over to a regime dominated by variable range hopping [VRH, $R = R_0 \exp(\frac{T_0}{T})^{0.5}$; see Fig. 1(a)] between 40 and 10 K, both for $\mu_0 H = 0\,\mathrm{T}$ (in the antiferromagnetic state of the material) and at $\mu_0 H = 2\,\mathrm{T}$ (in the spin-flip phase with all spins aligned). The activation energy E_a and characteristic hopping temperature T_0 decrease when a magnetic field is applied. We perform an analysis in terms of established theory for hopping transport and attribute the change in E_a to a 20 meV downshift of the conduction band edge and the reduction in T_0 to the possibility for the electrons to do shorter hops in the spin-aligned state. These conclusions show how the analysis of linear transport provides detailed information about the interplay of the magnetic state and microscopic

*alberto.morpurgo@unige.ch

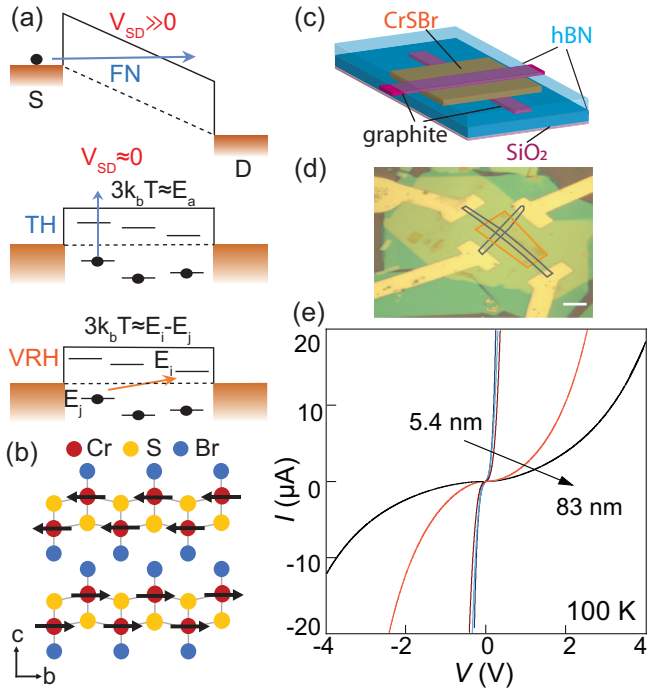

FIG. 1. (a) Schematic representation of possible vertical transport mechanisms. Band diagram of Fowler-Nordheim (FN) tunneling of electrons through a triangular potential barrier at high applied source-drain bias V_{sd}. At low applied bias—in the linear regime—electron transport occurs either via thermally activated hopping in the high-temperature regime (middle panel) or via variable range hopping (VRH) at lower temperatures (bottom panel). (b) Crystal structure of bilayer CrSBr viewed along the *a* axis. The red, blue, and yellow balls represent the Cr, Br, and S atoms, respectively. The black arrows represent the individual spins on the Cr atoms, showing the layered antiferromagnetic alignment within the material. (c) Schematic representation and (d) optical microscope image of one of the CrSBr devices employed in our experiments. The device consists of a CrSBr crystal [orange contour in (d)] placed between graphite contacts [gray contour in (d)] encapsulated with top and bottom hexagonal boron nitrite (hBN). The scale bar in (d) is 5 μm. (e) *I*-*V* characteristics of five different CrSBr devices, with thicknesses of 5.4, 5.4, 6.3, 53, and 83 nm, measured at 100 K.

electronic processes in van der Waals (vdW) magnetic semiconductors.

II. RESULTS AND ANALYSIS

CrSBr is a vdW layered antiferromagnetic semiconductor [see Fig. 1(b)] with a relatively large bandwidth within the layers [20,21] and Néel temperature of $T_N = 132$ K [20–23]. Its magnetic properties have been extensively characterized for both bulk and thin exfoliated layers, and it is established that, at low temperature, the application of a magnetic field of 2 T parallel to the *c* axis brings the material into the fully spin-polarized state [20–22]. The in-plane transport properties have also been carefully studied experimentally in bulk [22] and in field-effect transistors based on exfoliated crystals [21,24]. The conductivity of the material was found to remain high down to cryogenic temperatures, indicating that a large concentration of unintentional dopants (associated with defects in the material) is present and that the Fermi level is located very close to the conduction band edge. Although important aspects of the experimental results remain to be understood, such as the anomalous, gate dependent anisotropy in the conductivity, the temperature dependence of the electrical conductivity in bulk crystals is successfully reproduced by established theory for hopping transport, with thermally activated and variable range hopping regimes at high and low temperatures [21,24]. As for transport in the *c* direction (i.e., in the direction perpendicular to the layers), only experiments on mono- and bilayers, in which current is due to direct tunneling, have been reported [23].

Here, we investigate the processes mediating transport through crystals with thickness ranging from approximately 5 to 100 nm, using vertical junction devices in which an exfoliated layer is contacted on opposite sides with few-layer graphene strips [see Figs. 1(c) and 1(d)]. The high unintentional doping level of CrSBr crystals is ideal for generating a sufficiently high electrical hopping conductivity also along the *c* axis, enabling the linear transport regime to be accessed down to low temperature. Different from the in-plane electrical conductivity, transport in the *c* direction is mediated by electrons hopping between states in different layers that, depending on the magnetic state of the material, may have opposite magnetization. To properly model these interlayer hopping processes it is important to understand the nature of the defect states involved and the relation between their spin and the layer magnetization. This information was obtained in recently reported scanning tunneling microscopy and spectroscopy measurements [25], which revealed the presence of a large density of defects—mainly Br vacancies—that create states localized within individual layers, with energy close to the conduction band edge. Theoretical calculations within the same work [25] also showed that carriers in these localized states have their spin aligned with that of the layer magnetization, a conclusion consistent with the interpretation of several experiments reported in the literature [23,24,26]. We will refer back to the nature of the defect-induced states involved in the hopping process later, when we microscopically interpret the results of our measurements.

The CrSBr crystals employed in our work were grown by a chemical vapor transport method utilizing S_2Br_2 as a transport agent [21], and the devices were realized employing common pickup and transfer techniques [27], electron-beam lithography, electron-beam evaporation of Pt/Au, and liftoff (for details of the structure fabrication see Appendix A). We performed measurements on five different devices based on four different exfoliated crystals with different thicknesses between room temperature and 10 K (the precise range depends on multilayer thickness) and found a fully consistent temperature and magnetic field dependent behavior of the resistivity, which we illustrate with data measured on a device in which the CrSBr layer is 5.4 nm thick (data from other devices are shown in Appendixes A to C). The consistency of measurements performed on devices with different thicknesses is important not only to establish the reproducibility of the resistivity data but also to ensure that contact effects, which would make a more sizable contribution to the resistance in thinner devices, are not influencing the final results.

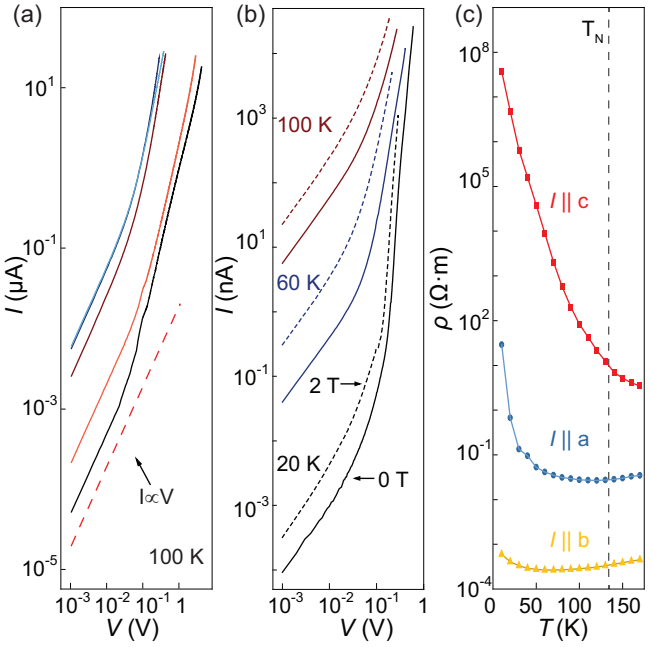

FIG. 2. (a) I-V characteristics measured at 100 K on five different CrSBr devices, with thicknesses of 5.4, 5.4, 6.3, 53, and 83 nm, plotted in double-logarithmic scale [same data as in Fig. 1(e) plotted for $V > 0$ V]. The red dashed line has a slope equal to 1, as expected for a linear I-V dependence. (b) I-V characteristics of a 5.4 nm thick device measured at 20, 60, and 100 K; the solid and dashed lines correspond to measurements performed at $\mu_0 H = 0$ T (in the antiferromagnetic phase of CrSBr) and at $\mu_0 H = 2$ T (in the fully spin-polarized phase). (c) Temperature dependence of the linear resistivity of CrSBr measured along the a, b, and c directions (the resistivity in the a and b directions is reproduced from our earlier study of CrSBr field-effect transistors [21], where we showed that the a (b) direction corresponds to the long (short) lateral side of the exfoliated crystals).

Figure 1(e) shows the I-V characteristics of the five devices studied, measured at $T = 100$ K, with all exhibiting a clear nonlinearity as the bias is increased. We identify the linear regime by plotting the I-V characteristics on a double-logarithmic scale [Fig. 2(a)] and selecting the low-bias part of the curve with slope equal to 1. As expected, in all devices current in this regime rapidly decreases (and the onset of the nonlinearity shifts to lower applied voltage) as temperature is lowered. Also, in all devices the application of a magnetic field of 2 T, which is sufficient to enter the spin-flip phase of CrSBr, leads to a current increase at all temperatures and biases [see Fig. 2(b)].

We start our analysis by looking at the magnitude of the linear resistivity and estimate the electronic anisotropy by comparing the value of the resistivity in the c direction to that in the a and b directions, measured earlier using field-effect transistor devices (we take the value of the resistivity measured at zero gate voltage) [21]. At low temperature, the resistivity in the c direction is approximately 11 orders of magnitude larger than in the b direction and 6–8 orders of magnitude larger than the conductivity in the a direction [the exact value depends on the device from which the values of the a and b resistivities are extracted; see Fig. 2(c)]. This giant anisotropy is consistent with the bandwidth in the three different directions, as obtained from *ab initio* calculations [see Figs. 4(a) and 4(b) below]. Specifically, in the antiferromagnetic state, the dispersion in the Γ-Z direction (i.e., the c direction) shows a bandwidth of only a few meV, much smaller than the bandwidth in the other two directions (Γ-X and Γ-Y), corresponding, respectively, to the a and b directions, i.e., to in-plane motion within the material layers. The anisotropy inferred from the resistivity measured in the c direction is extremely large, much larger than in any other van der Waals material that we know of [28], and implies a very small electronic coupling between adjacent layers of CrSBr.

We then analyze the evolution of the resistance as a function of T in terms of established theory for hopping transport in disordered semiconductors. When the Fermi level is in the tail of states below the conduction band edge, theory predicts the resistance to exhibit a thermally activated behavior $R \propto \exp(\frac{E_a}{kT})$ at sufficiently high temperature [see Fig. 1(a)] [29]. The value of E_a may be determined by the energy distribution of localized states in the band tail or by the distance between the Fermi level E_F and the conduction band edge (as electrons may have enough energy to hop from a localized state into the conduction band and propagate before being trapped again). At lower temperatures, transport should cross over to a VRH regime, in which $R \propto \exp(\frac{T_0}{T})^p$ [see Fig. 1(a)], with p determined by the electronic dimensionality, influence of Coulomb repulsion, and other details [29,30].

Figure 3(a) shows the evolution of the resistance upon cooling, starting from 200 K (other devices were measured from up to 290 K; see Appendix C). As expected, between 200 and 60 K $\ln(R)$ depends linearly on $1/T$ [see Fig. 3(b)], with a change in slope for $T > T_N$ (in the paramagnetic state) and $T < T_N$ [in the layered antiferromagnetic state; see blue and black lines in Fig. 3(b)]. Additionally, for $T < T_N$, the resistance continues to exhibit a thermally activated behavior also in the presence of a perpendicular magnetic field $\mu_0 H = 2$ T, which is larger than the spin-flip field for all temperatures, with an activation energy in the spin-flip phase that is smaller than in the antiferromagnetic state [see red line in Fig. 3(b)]. Linear fits to the data allow the activation energy to be extracted in all different conditions. For this device, we find $E_a = 42$ meV for T between 200 K and T_N (i.e., in the paramagnetic state) and $E_a = 74$ and 56 meV for T between T_N and 60 K without and with a 2 T applied magnetic field, respectively. These values are comparable to those found in other devices (see Table I and Appendix A for details about the different devices), from which we estimate an average $E_a = 46 \pm 9$ meV in the paramagnetic (PM) state, $E_a = 79 \pm 6$ meV in the antiferromagnetic (AFM) state, and $E_a = 59 \pm 4$ meV in the spin-flip phase at $\mu_0 H = 2$ T [i.e., the ferromagnetic (FM) state].

The quantitative analysis of the resistance in the VRH regime, with $R \propto \exp(T_0/T)^p$, depends on the exponent p in the exponential. For isotropic materials theory predicts $p = 1/(D+1)$ (where D is the system dimensionality) if electron-electron interactions can be neglected (Mott regime) and $p = 1/2$ irrespective of D if electron-electron interaction dominate [Efros-Skhlovskii (ES) regime]. Here, we select $p = 1/2$ because the range of temperatures in which the VRH regime is observed, well below 100 K, corresponds to

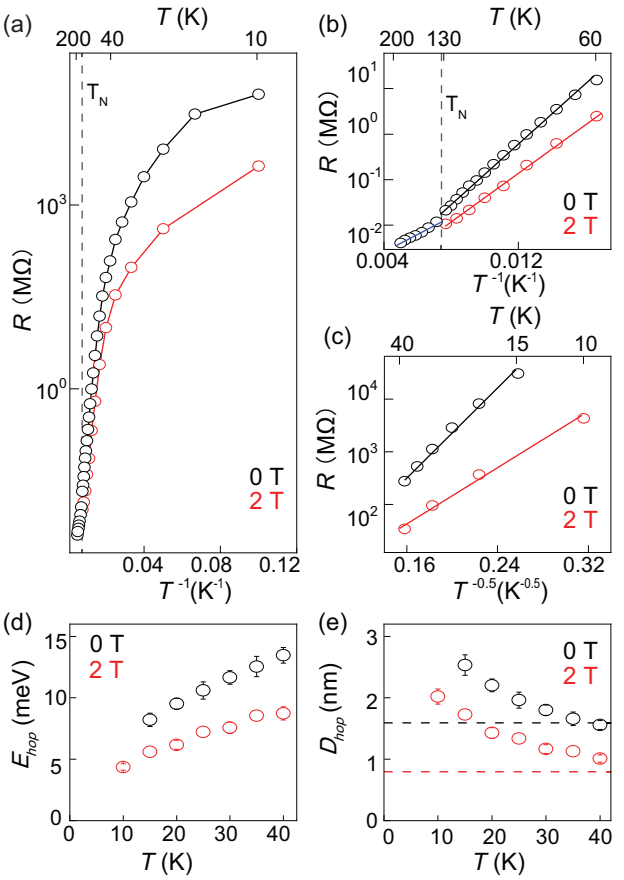

FIG. 3. (a) Resistance of a 5.4 nm thick CrSBr device as a function of $1/T$, measured at $\mu_0 H = 0$ T (black symbols) and 2 T (red symbols; $H \parallel c$) in the full temperature range, covering the thermally activated and variable range hopping regimes. (b) Resistance as a function of $1/T$, focusing on the thermally activated regime between 60 and 200 K. The different symbols correspond to the paramagnetic (blue), antiferromagnetic (black), and spin-flip (red) states of the material (the solid lines of the corresponding color are linear fits to the data). (c) Resistance as a function of $T^{-0.5}$ in the variable range hopping regime between 40 and 10 K in the antiferromagnetic (black symbols) and spin-flip (red symbols) states at $\mu_0 H = 0$ and 2 T, respectively. The solid lines are linear fits to the data. The analysis of transport in the variable range hopping regime in the temperature range between 10 and 40 K gives, through Eqs. (1) and (2), (d) the mean hopping energy $E_{\rm hop}$ and (e) the mean hopping distance $D_{\rm hop}$. Black and red symbols correspond to the average values of these quantities (from all devices) extracted from the antiferromagnetic state of CrSBr at $\mu_0 H = 0$ T and in the fully spin-polarized spin-flip phase at $\mu_0 H = 2$ T (see Appendix C for data from different devices). In (e), the dashed horizontal lines represent the distance between two adjacent layers (red dashed line) and to the next-nearest layer (black dashed line), which correspond to the shortest possible hopping distance in the fully polarized spin-flip state and in the antiferromagnetic state of CrSBr.

characteristic energies smaller than 10 meV, and on this energy scale it should certainly be expected that electron-electron interactions play a role in a layered van der Waals semiconductor. Figure 3(c) shows that the relation between $\ln(R)$ and $1/T^{1/2}$ is, indeed, linear between 40 and 10 K, both

TABLE I. Overview of hopping transport parameters: the activation energy and T_0 value for all measured devices in the different magnetic states.

	Device					Average
	A1	A2	B	C	D	value
Thickness (nm)	5.4	5.4	6.3	53	83	
E_a, AFM (meV)	74	71	80	85	84	79
E_a, FM (meV)	56	57	58	67	58	59
E_a, PM (meV)	42	35	54	56	43	46
T_0, AFM (K)	2209	2663		2490		2454
T_0, FM (K)	894	1122		1075		1030

in the antiferromagnetic state (black line) and in the spin-flip phase with 2 T applied magnetic field (red line). The values of T_0 are extracted by determining the slope, from which we obtain $T_0(B = 0\ T) = 2209$ K and $T_0(B = 2\ T) = 894$ K (see Table I for the fitting results for the other devices).

As the values of T_0 give little physical intuition, we resort to VRH theory to relate T_0 to quantities that have a direct physical interpretation. These are the average change in energy of an electron upon hopping $E_{\rm hop}$ and the mean distance in a hopping process $D_{\rm hop}$. Within ES theory [29,30], these quantities read

$$E_{\rm hop} = \frac{1}{2} k T^{\frac{1}{2}} T_0^{\frac{1}{2}}, \tag{1}$$

$$D_{\rm hop} = \frac{1}{4} a \left(\frac{T_0}{T}\right)^{\frac{1}{2}}. \tag{2}$$

Here, k is the Boltzmann constant, and a is the localization length (i.e., the spatial extension of the localized states). To proceed with a quantitative analysis, we need to establish the value of a. To this end we recall that the localized states involved in the hopping processes originate from defects (mainly bromine vacancies) in individual layers, whose wave functions are also localized within individual layers (i.e., the overlap of states in neighboring layers is small). The very high resistivity in the c direction observed in the experiments is a direct consequence of the small overlap of wave functions in different layers, the same reason why the width of the CrSBr bands in the c direction is extremely narrow. As the defect states mediating the hopping processes are localized within the individual layers and only very weakly coupled, we can take as the value for the localization length a the distance between two adjacent layers (i.e., $a = 0.8$ nm)

The values of $E_{\rm hop}$ and $D_{\rm hop}$ extracted from different devices are very close to each other irrespective of the thickness of the CrSBr layer. Figures 3(d) and 3(e) show the temperature dependence of these quantities plotted from Eqs. (1) and (2), using for T_0 the average of the values obtained experimentally from all devices measured. $E_{\rm hop}$ scales approximately linearly with T throughout the range in which VRH properly describes transport. $E_{\rm hop} \approx 4$–9 meV in the spin-polarized state and is somewhat larger in the antiferromagnetic state. Finding a value just slightly larger than the thermal energy (i.e., $\simeq 3.5 k_B T$) should be expected and confirms the soundness of the analysis. The hopping distance $D_{\rm hop}$ at the onset of VRH ($T = 40$ K) is close to 1 nm (comparable to the interlayer

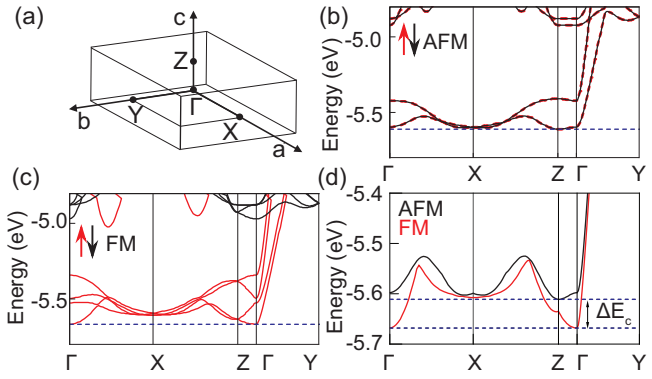

FIG. 4. (a) Brillouin zone and high-symmetry paths along which the bands are shown in the band structure calculations of (b) antiferromagnetic and (c) ferromagnetic states in the CrSBr bulk. The crystallographic a, b, and c axes correspond to the Γ-X, Γ-Y, and Γ-Z directions, respectively. The bandwidth along Γ-Z is clearly smaller than in the other two directions. The horizontal dark blue dashed lines in (b) and (c) represent the bottom of the conduction band. (d) Comparison of the conduction band edge position in the antiferromagnetic and ferromagnetic states. A downshift of the conduction band edge ($\bigtriangleup E_C \approx 50$ meV) occurs when going from the antiferromagnetic state to the ferromagnetic state.

separation of 0.8 nm, as illustrated by the red dashed line) in the spin-polarized state and is twice the value in the antiferromagnetic state (black dashed line). For both states, D_{hop} increases slightly upon cooling from 40 to 15 K as electrons have to jump farther to find states with appropriate energy (see also discussion below).

Before discussing the microscopic interpretation of these findings, we note that these results also indicate the consistency of the $p = 0.5$ value selected for the VRH analysis. Indeed, we analyzed the data with smaller p values and found larger hopping distances. For instance for $p = 0.25$, D_{hop} turns out to be larger than the thickness of our thinnest device (5.4 nm), a conclusion not internally consistent since it would imply that electrons can tunnel directly through the entire multilayer and transport would not be in the hopping regime (and should therefore not show hopping temperature dependence).

The 20 meV decrease in activation energy E_a observed when passing from the antiferromagnetic to the spin-polarized state of CrSBr, as well as the change in T_0 (with the corresponding change in D_{hop} inferred from the analysis of hopping transport), results from the interplay between the magnetic state of CrSBr and electronic transport. As for E_a, *ab initio* calculations (see Fig. 4) do, indeed, predict that in the ferromagnetic state the conduction band edge is downshifted by a few tens of meV [see Fig. 4(d); the exact value depends on the thickness of the multilayer considered]. The lower energy of the conduction band edge explains the lowering of the activation energy measured in the presence of a 2 T applied field (which brings CrSBr into the spin-flip phase with all spin aligned) and captures the correct order of magnitude of the effect. Note that a comparable magnitude downshift of the conduction band edge between the antiferromagnetic and the spin-flip phase was also recently found in $CrPS_4$, another 2D layered antiferromagnetic semiconductor, both theoretically and experimentally [31,32]. Our findings on CrSBr therefore suggest that a downshift of the conduction band is a common property of these layered antiferromagnetic materials.

The reason T_0 changes when passing from the antiferromagnetic phase to the spin-flip phase can be easily understood if we consider the corresponding change in average hopping distance. As discussed above, the defects states involving in the hopping process have their spin aligned with the magnetization of the layer hosting them. In the antiferromagnetic state, therefore, electrons in one layer cannot hop to the nearest adjacent layers because the large exchange energy [approximately 0.6 eV according to *ab initio* calculations; see Fig. 4(c)] shifts states with the same spin to much larger energy values and makes them energetically inaccessible. As a result, the shortest hop possible in the c direction in the antiferromagnetic state is to the second-next layer. In contrast, in the spin-polarized state hopping to the next layer is unimpeded. That is why the typical hopping distance at $\mu_0 H = 2$ T (i.e., in the spin-flip phase) corresponds to the thickness of a single monolayer and at $\mu_0 H = 0$ T in the antiferromagnetic state is twice as long. This is, indeed, what is quite precisely observed at the largest temperature of the VRH range hopping regime, when electrons have enough energy to find the closest possible state to hop to. As T is lowered, the hopping distance increases while remaining the same order of magnitude because electrons need to do hops over a somewhat longer distance because the hopping sites with suitable energy in nearby layers are displaced laterally relative to each other (i.e., in general, defects in nearby layers are shifted relative to each other).

III. CONCLUSIONS

We conclude that the analysis of hopping transport in the direction perpendicular to the layers in CrSBr barriers provides detailed insight into the nature of the microscopic processes responsible for electronic motion in a layered antiferromagnetic semiconductor. In particular, the evolution with magnetic field of the thermally activated and variable range hopping regimes reveals how layered antiferromagnetism influences both the conduction band in reciprocal space and electronic motion in real space. It is certainly worth emphasizing that it is the possibility to analyze transport in terms of an established theory—the theory of hopping transport through disordered semiconductors—that allows extracting precise and quantitatively reliable information about the interplay of electron dynamics and the magnetic state of the material.

ACKNOWLEDGMENTS

The authors gratefully acknowledge A. Ferreira for continuous and valuable technical support. We thank M. Liao and N. Ubrig for fruitful discussions. A.F.M. acknowledges financial support from the Swiss National Science Foundation under Project No. 200020_178891 and the EU Graphene Flagship project for support. M.G. acknowledges support from Ministero dell'Università e della Ricerca through the PNRR project ECS_00000033_ECOSISTER. F.O.v.R. acknowledges financial support from the Swiss National Science Foundation under Grant No. PCEFP2_194183.

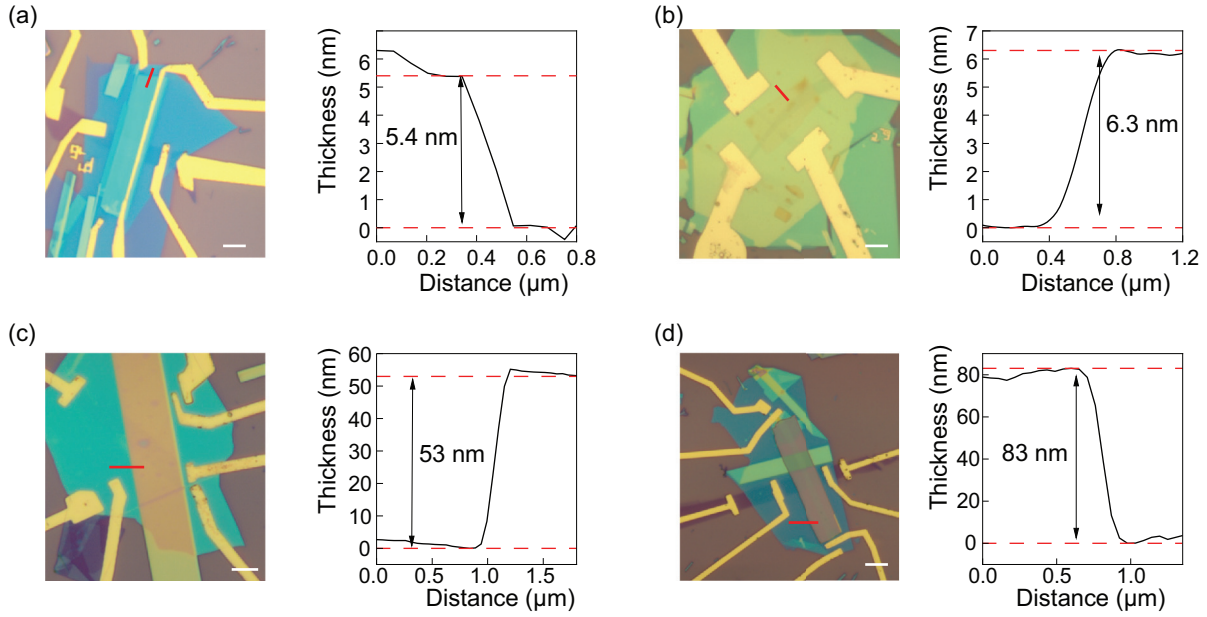

FIG. 5. Optical microscope images (left panels) and height profiles extracted from atomic force microscopy measurements (right panels; each profile is measured along the red dashed line traces shown in the left panel) for devices (a) A1/A2, (b) B, (c) C, and (d) D. In all microscope images the scale bar is 5 μm.

APPENDIX A: METHODS

1. First-principles calculations

In Figures 4(b)–4(d) of the main text we show the calculated band structure of CrSBr in the layered antiferromagnetic state and in the fully spin-aligned (ferromagnetic) state. The band structure is obtained by first-principles density-functional theory calculations using the QUANTUM ESPRESSO distribution [33,34]. van der Waals interactions have been included by adopting the spin-polarized extension [35] of the revised vdw-DF3-opt2 exchange-correlation functional [36], with pseudopotentials from the standard solid-state pseudopotential (SSSP) accuracy library (version 1.0) [37,38] with energy cutoffs of 40 and 320 Ry for wave functions and density, respectively. A uniform $12 \times 9 \times 4$ mesh of k points corresponding to a Γ-centered Monkhorst-Pack grid was used in self-consistent calculations. Atomic positions and lattice parameters were fully relaxed within the antiferromagnetic configuration (with doubled unit cell in the vertical direction) using a Broyden-Fletcher-Goldfarb-Shanno (BFGS) algorithm until the residual force on each atom was below 2.6 meV/Å and each component of stress was below 0.5 kbar, which gives lattice parameters in good agreement with experiments ($a = 3.52$ Å, $b = 4.71$ Å, $c = 15.96$ Å). For a better comparison with the antiferromagnetic case, the same doubled unit cell was also adopted for band structure calculations in the ferromagnetic configuration. Energy bands in the two magnetic configurations were aligned so that the energies of the deepest semicore states match.

2. Device fabrication

The vertical junction devices investigated in this work were fabricated using 5.4 nm (A1 and A2), 6.3 nm (B), 53 nm (C), and 83 nm (D) thick CrSBr crystals (see Fig. 5 for atomic force microscope profiles), exfoliated from bulk crystals grown in house by means of chemical vapor transport (see Ref. [21] for details on the crystal growth and characterization). Although CrSBr does not exhibit signs of degradation when exposed to ambient conditions for short periods of time, the devices were assembled in a nitrogen-gas-filled glove box with oxygen and water concentration below parts per million, using established pickup and transfer techniques (the substrates are made of silicon covered with 285 nm SiO_2). The device structure consists of exfoliated multilayer graphene top and bottom contacts placed over a bottom hexagonal boron nitrite (hBN) layer (in device B we also added a top hBN layer to encapsulate the exfoliated CrSBr crystal completely, and no significant differences in the transport properties were observed compared to the nonencapsulated devices). The Pt/Au leads connected to the multilayer graphene contacts were fabricated via standard electron-beam lithography and evaporation followed by liftoff (in device B the connection to the multilayer graphene electrode was made via Cr/Au edge contacts using reactive ion etching with a CF_4/O_2 mixture prior to metal deposition).

Finally, junction A1 and junction A2 (see Fig. 5 for optical images of the devices) are realized on the same CrSBr exfoliated crystals but with different contact configurations. Specifically, the bottom graphene contact is shared by the two junctions, but the top contact is different in the two cases: it consists of graphene for junction A1 and of a Pt film directly evaporated on top of CrSBr for junction A2. This configuration allows us to compare two devices realized on the same CrSBr crystal with different contacts, which is useful for confirming that the contact resistance is not determining the behavior observed experimentally. Indeed, as discussed in Appendix B, the contact material has no influence on the linear regime of the current-voltage (I-V) characteristics of the devices.

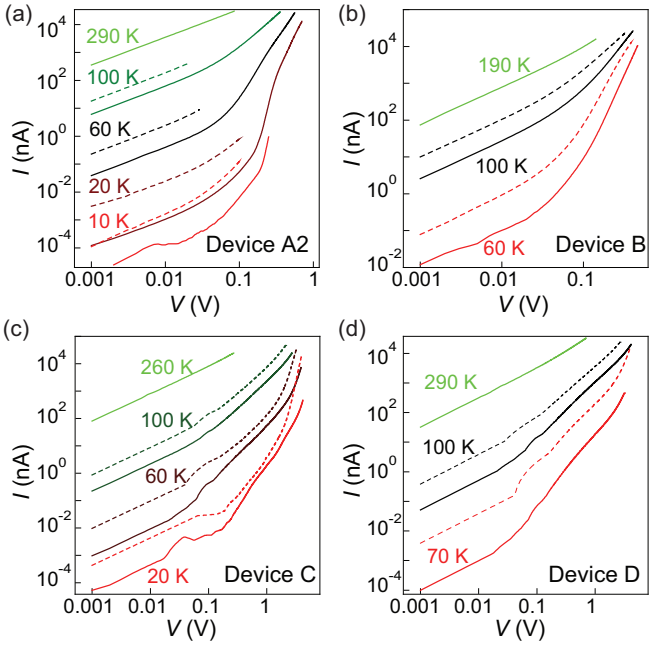

FIG. 6. I-V curves of devices (a) A2, (b) B, (c) C, and (d) D plotted in double-logarithmic scale, measured at different temperatures (as indicated next to each curve) and magnetic fields (the solid and dashed lines correspond to data measured at $\mu_0 H = 0T$ and $\mu_0 H = 2T$).

3. Electronic transport measurements

Transport measurements were performed using a Teslatron Cryogen-free II cryostat (Oxford Instruments) equipped with a variable temperature insert, allowing us to stabilize the temperature at any value between room temperature and 1.7 K. A 12 T superconducting magnet was used to apply magnetic field. Electrical measurements were performed in a four-terminal voltage bias configuration using a homemade voltage source and low-noise current/voltage amplifiers connected to digital multimeters (Keysight 34401A).

APPENDIX B: I-V CHARACTERISTICS OF CrSBr MULTILAYERS

As discussed in the main text, the investigation of thermally activated transport and variable range hopping (VRH) relies on the observation of the linear transport regime in the current-voltage (I-V) characteristics of our devices. In the main text we mostly show data for device A1. Here, we show that the linear transport regime can be detected in all the investigated devices, as illustrated in Fig. 6, which presents the I-V characteristics of devices A2, B, C, and D on a double-logarithmic scale. Except for device D, whose resistance in the linear regime was too large to measure below 40 K, and device B, which broke at 60 K, the linear regime was investigated down to 10 K at both 0 T and 2 T (sufficient to bring CrSBr into the spin-flip phase, in which all the spins are aligned parallel to the applied field). In summary, thermally activated transport was measured on all five devices realized, and the variable range hopping regime was studied in three out of five devices.

As mentioned above, we also compared the I-V characteristics of devices A1 and A2 realized on the same CrSBr crystal

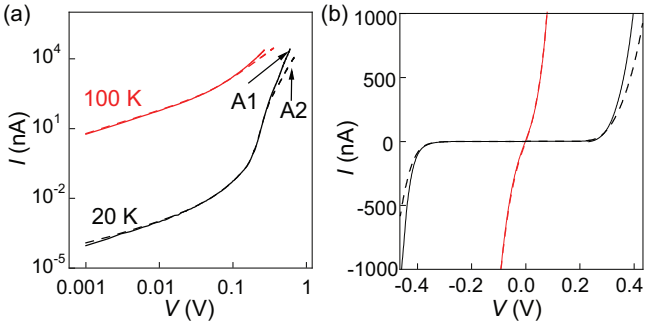

FIG. 7. (a) Double-logarithmic- and (b) linear-scale I-V characteristic of graphene/CrSBr/graphene (A1) and graphite/CrSBr/Pt (A2) devices realized on the same CrSBr multilayer (the solid and dashed lines represent data from devices A1 and A2, respectively). Positive bias corresponds to injecting electrons from the top electrode (multilayer graphene for device A1 and Pt for device A2), and negative bias corresponds to injecting electrons from the common bottom multilayer graphene electrode. Data are taken at zero applied magnetic field.

with different contacts (see Appendix A for details) to ensure that any effect of the contact resistance on our measurements is negligible (i.e., our experiments really probe the electronic properties of CrSBr and not the interface with the metal contacts). As can be seen in Fig. 7, the I-V curves measured in the two junctions perfectly fall on top of each other in the linear regime and start to deviate slightly only at larger applied bias, when the devices are biased outside the linear regime. This observation, together with the reproducibility of all measured

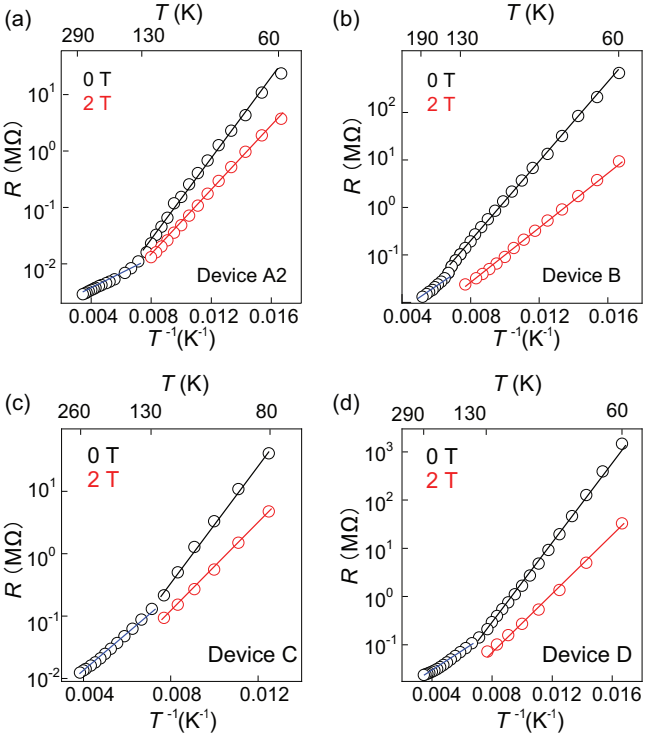

FIG. 8. Arrhenius plots of resistance as a function of inverse temperature for devices (a) A2, (b) B, (c) C, and (d) D. The black, red, and blue lines represent linear fits to the data in the antiferromagnetic, spin-flip, and paramagnetic states, respectively.

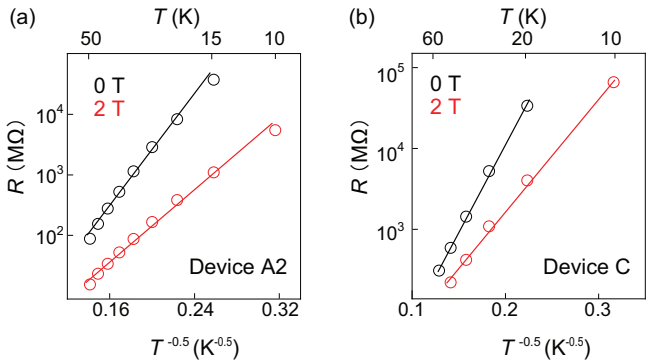

FIG. 9. Semilogarithmic plot of the resistance versus $T^{-0.5}$ for devices (a) A2 and (b) C. The black and red lines represent linear fits to the data with applied magnetic field $\mu_0 H = 0$ and 2 T.

quantities (resistivity, activation energy, T_0) in devices whose thickness ranges from 5 to nearly 100 nm, fully confirms that our measurements of transport in the linear regime do probe the properties of CrSBr and are not affected by the contact resistance.

APPENDIX C: ANALYSIS OF ACTIVATION ENERGY E_a AND CHARACTERISTIC TEMPERATURE T_0 FOR DIFFERENT DEVICES

As shown in the main text, the analysis of the resistance extracted from the linear regime revealed the presence of thermally activated behavior from 200 to 60 K, followed by VRH from 40 to 10 K, with the exact temperature range depending slightly on the investigated device. In the main text we show data from device A1. For completeness, here, we show the data measured on all our devices, which we used to extract the average activation energy E_a and characteristic temperature T_0 reported in the main text and summarized in Table I.

Figure 8 shows the Arrhenius plots obtained for devices A2, B, C, and D in the paramagnetic (290 to 140 K, 0 T), antiferromagnetic (130 to 60 K, 0 T) and spin-flip (130 to 60 K, 2 T) phases. Figure 9 shows a plot of $\ln(R)$ and $1/T^{1/2}$ (corresponding to the Efros-Skhlovskii VRH regime) between

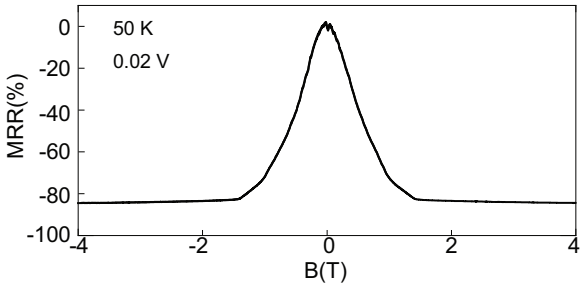

FIG. 10. Magnetoresistance $[R(B) - R(B = 0)]/R(B = 0)$ measured on device A2 at $T = 50$ K with an applied bias of $V = 0.02$ V (corresponding to having the device biased in the linear part of the I-V curve). The magnetic field is parallel to the c axis.

50 and 10 K in the antiferromagnetic state (0 T) and spin-flip phase (2 T) for devices A2 and C. The values of E_a extracted from linear fits of $\ln(R)$ vs $1/T$ as well as the values of T_0 extracted from linear fits of $\ln(R)$ vs $1/T^{1/2}$ in the different magnetic states are summarized in Table I.

APPENDIX D: MAGNETOTRANSPORT IN THE LINEAR TRANSPORT REGIME

In the main text, we show the analysis of temperature-dependent resistance both at $\mu_0 H = 0$ T (i.e., in the antiferromagnetic state of CrSBr) and at $\mu_0 H = 2$ T (i.e., in the spin-flip state, with all spin pointing in the same direction). For completeness, here, we show magnetoresistance data measured at 50 K in the linear part of the I-V curve after varying the applied perpendicular magnetic field from -4 to 4 T. As shown in Fig. 10, a continuously varying magnetoresistance $[R(B) - R(B = 0)]/R(B = 0)$ is observed, whose magnitude corresponds approximately to a factor of 2 change in resistance. The magnetoresistance is clearly seen to saturate when the applied magnetic field exceeds the spin-flip field (close to 1.5 T). Finding that the resistance decreases upon applying magnetic field to align the magnetization in all of layers is typical for vertical transport through A-type antiferromagnetic semiconductors, irrespective of the transport regime.

[1] K. S. Burch, D. Mandrus, and J.-G. Park, Magnetism in two-dimensional van der Waals materials, Nature (London) **563**, 47 (2018).

[2] M. Gibertini, M. Koperski, A. F. Morpurgo, and K. S. Novoselov, Magnetic 2D materials and heterostructures, Nat. Nanotechnol. **14**, 408 (2019).

[3] K. F. Mak, J. Shan, and D. C. Ralph, Probing and controlling magnetic states in 2D layered magnetic materials, Nat. Rev. Phys. **1**, 646 (2019).

[4] Z. Wang, M. Gibertini, D. Dumcenco, T. Taniguchi, K. Watanabe, E. Giannini, and A. F. Morpurgo, Determining the phase diagram of atomically thin layered antiferromagnet $CrCl_3$, Nat. Nanotechnol. **14**, 1116 (2019).

[5] G. Long, H. Henck, M. Gibertini, D. Dumcenco, Z. Wang, T. Taniguchi, K. Watanabe, E. Giannini, and A. F. Morpurgo, Persistence of magnetism in atomically thin $MnPS_3$ crystals, Nano Lett. **20**, 2452 (2020).

[6] C. Gong, L. Li, Z. Li, H. Ji, A. Stern, Y. Xia, T. Cao, W. Bao, C. Wang, Y. Wang, Z. Q. Qiu, R. J. Cava, S. G. Louie, J. Xia, and X. Zhang, Discovery of intrinsic ferromagnetism in two-dimensional van der Waals crystals, Nature (London) **546**, 265 (2017).

[7] B. Huang, G. Clark, E. Navarro-Moratalla, D. R. Klein, R. Cheng, K. L. Seyler, D. Zhong, E. Schmidgall, M. A. McGuire, D. H. Cobden, W. Yao, D. Xiao, P. Jarillo-Herrero, and X. Xu, Layer-dependent ferromagnetism in a van der Waals crystal down to the monolayer limit, Nature (London) **546**, 270 (2017).

[8] D. R. Klein, D. MacNeill, J. L. Lado, D. Soriano, E. Navarro-Moratalla, K. Watanabe, T. Taniguchi, S. Manni, P. Canfield, J. Fernández-Rossier, and P. Jarillo-Herrero, Probing magnetism

in 2D van der Waals crystalline insulators via electron tunneling, Science **360**, 1218 (2018).

[9] T. Song, X. Cai, M. W.-Y. Tu, X. Zhang, B. Huang, N. P. Wilson, K. L. Seyler, L. Zhu, T. Taniguchi, K. Watanabe, M. A. McGuire, D. H. Cobden, D. Xiao, W. Yao, and X. Xu, Giant tunneling magnetoresistance in spin-filter van der Waals heterostructures, Science **360**, 1214 (2018).

[10] H. H. Kim, B. Yang, T. Patel, F. Sfigakis, C. Li, S. Tian, H. Lei, and A. W. Tsen, One million percent tunnel magnetoresistance in a magnetic van der Waals heterostructure, Nano Lett. **18**, 4885 (2018).

[11] Z. Wang *et al.*, Electric-field control of magnetism in a few-layered van der Waals ferromagnetic semiconductor, Nat. Nanotechnol. **13**, 554 (2018).

[12] H. H. Kim, B. Yang, S. Tian, C. Li, G.-X. Miao, H. Lei, and A. W. Tsen, Tailored tunnel magnetoresistance response in three ultrathin chromium trihalides, Nano Lett. **19**, 5739 (2019).

[13] T. Song, Z. Fei, M. Yankowitz, Z. Lin, Q. Jiang, K. Hwangbo, Q. Zhang, B. Sun, T. Taniguchi, K. Watanabe, M. A. McGuire, D. Graf, T. Cao, J.-H. Chu, D. H. Cobden, C. R. Dean, D. Xiao, and X. Xu, Switching 2D magnetic states via pressure tuning of layer stacking, Nat. Mater. **18**, 1298 (2019).

[14] Z. Wang, I. Gutiérrez-Lezama, D. Dumcenco, N. Ubrig, T. Taniguchi, K. Watanabe, E. Giannini, M. Gibertini, and A. F. Morpurgo, Magnetization dependent tunneling conductance of ferromagnetic barriers, Nat. Commun. **12**, 6659 (2021).

[15] D. Soler-Delgado, F. Yao, D. Dumcenco, E. Giannini, J. Li, C. A. Occhialini, R. Comin, N. Ubrig, and A. F. Morpurgo, Probing magnetism in exfoliated VI_3 layers with magnetotransport, Nano Lett. **22**, 6149 (2022).

[16] R. H. Fowler and L. Nordheim, Electron emission in intense electric fields, Proc. R. Soc. London, Ser. A **119**, 173 (1928).

[17] M. Lenzlinger and E. Snow, Fowler-Nordheim tunneling into thermally grown SiO_2, J. Appl. Phys. **40**, 278 (1969).

[18] H. Wang, V. Eyert, and U. Schwingenschlögl, Electronic structure and magnetic ordering of the semiconducting chromium trihalides $CrCl_3$, $CrBr_3$, and CrI_3, J. Phys.: Condens. Matter **23**, 116003 (2011).

[19] Y. Zheng, X.-X. Jiang, X.-X. Xue, J. Dai, and Y. Feng, *Ab initio* study of pressure-driven phase transition in $FePS_3$ and $FePSe_3$, Phys. Rev. B **100**, 174102 (2019).

[20] N. P. Wilson, K. Lee, J. Cenker, K. Xie, A. H. Dismukes, E. J. Telford, J. Fonseca, S. Sivakumar, C. Dean, T. Cao, X. Roy, X. Xu, and X. Zhu, Interlayer electronic coupling on demand in a 2D magnetic semiconductor, Nat. Mater. **20**, 1657 (2021).

[21] F. Wu, I. Gutiérrez-Lezama, S. A. López-Paz, M. Gibertini, K. Watanabe, T. Taniguchi, F. O. von Rohr, N. Ubrig, and A. F. Morpurgo, Quasi-1D electronic transport in a 2D magnetic semiconductor, Adv. Mater. **34**, 2109759 (2022).

[22] E. J. Telford, A. H. Dismukes, K. Lee, M. Cheng, A. Wieteska, A. K. Bartholomew, Y. Chen, X. Xu, A. N. Pasupathy, X. Zhu, C. R. Dean, and X. Roy, Layered antiferromagnetism induces large negative magnetoresistance in the van der Waals semiconductor CrSBr, Adv. Mater. **32**, 2003240 (2020).

[23] C. Boix-Constant, S. Mañas-Valero, A. M. Ruiz, A. Rybakov, K. A. Konieczny, S. Pillet, J. J. Baldoví, and E. Coronado, Probing the spin dimensionality in single-layer CrSBr van der Waals heterostructures by magneto-transport measurements, Adv. Mater. **34**, 2204940 (2022).

[24] E. J. Telford, A. H. Dismukes, R. L. Dudley, R. A. Wiscons, K. Lee, D. G. Chica, M. E. Ziebel, M.-G. Han, J. Yu, S. Shabani, A. Scheie, K. Watanabe, T. Taniguchi, D. Xiao, Y. Zhu, A. N. Pasupathy, C. Nuckolls, X. Zhu, C. R. Dean, and X. Roy, Coupling between magnetic order and charge transport in a two-dimensional magnetic semiconductor, Nat. Mater. **21**, 754 (2022).

[25] J. Klein, Z. Song, B. Pingault, F. Dirnberger, H. Chi, J. B. Curtis, R. Dana, R. Bushati, J. Quan, L. Dekanovsky, Z. Sofer, A. Alù, V. M. Menon, J. S. Moodera, M. Lončar, P. Narang, and F. M. Ross, Sensing the local magnetic environment through optically active defects in a layered magnetic semiconductor, ACS Nano **17**, 288 (2023).

[26] S. A. López-Paz, Z. Guguchia, V. Y. Pomjakushin, C. Witteveen, A. Cervellino, H. Luetkens, N. Casati, A. F. Morpurgo, and F. O. von Rohr, Dynamic magnetic crossover at the origin of the hidden-order in van der Waals antiferromagnet CrSBr, Nat. Commun. **13**, 4745 (2022).

[27] J. Deng, J. Guo, H. Hosono, T. Ying, and X. Chen, Two-dimensional bipolar ferromagnetic semiconductors from layered antiferromagnets, Phys. Rev. Mater. **5**, 034005 (2021).

[28] S. Najmaei, M. R. Neupane, B. M. Nichols, R. A. Burke, A. L. Mazzoni, M. L. Chin, D. A. Rhodes, L. Balicas, A. D. Franklin, and M. Dubey, Cross-plane carrier transport in van der Waals layered materials, Small **14**, 1703808 (2018).

[29] B. I. Shklovskii and A. L. Efros, *Electronic Properties of Doped Semiconductors*, Springer Series in Solid-State Sciences Vol. 45 (Springer, Springer Berlin, Heidelberg, 2013).

[30] M. Pollak and B. Shklovskii, *Hopping Transport in Solids* (Elsevier, Amsterdam, The Netherlands, 1991).

[31] F. Wu, M. Gibertini, K. Watanabe, T. Taniguchi, I. Gutiérrez-Lezama, N. Ubrig, and A. F. Morpurgo, Gate-controlled magnetotransport and electrostatic modulation of magnetism in 2D magnetic semiconductor $CrPS_4$, Adv. Mater. **35**, 2211653 (2023).

[32] F. Wu, M. Gibertini, K. Watanabe, T. Taniguchi, I. Gutiérrez-Lezama, N. Ubrig, and A. F. Morpurgo, Magnetism-induced band-edge shift as mechanism for magnetoconductance in $CrPS_4$ transistors, Nano Lett. **23**, 8140 (2023).

[33] P. Giannozzi *et al.*, QUANTUM ESPRESSO: A modular and open-source software project for quantum simulations of materials, J. Phys.: Condens. Matter **21**, 395502 (2009).

[34] P. Giannozzi *et al.*, Advanced capabilities for materials modelling with Quantum ESPRESSO, J. Phys.: Condens. Matter **29**, 465901 (2017).

[35] T. Thonhauser, S. Zuluaga, C. A. Arter, K. Berland, E. Schröder, and P. Hyldgaard, Spin signature of nonlocal correlation binding in metal-organic frameworks, Phys. Rev. Lett. **115**, 136402 (2015).

[36] D. Chakraborty, K. Berland, and T. Thonhauser, Next-generation nonlocal van der Waals density functional, J. Chem. Theory Comput. **16**, 5893 (2020).

[37] G. Prandini, A. Marrazzo, I. E. Castelli, N. Mounet, and N. Marzari, Precision and efficiency in solid-state pseudopotential calculations, npj Comput. Mater. **4**, 72 (2018).

[38] K. F. Garrity, J. W. Bennett, K. M. Rabe, and D. Vanderbilt, Pseudopotentials for high-throughput DFT calculations, Comput. Mater. Sci. **81**, 446 (2014).